Collective Dynamics in a Binary Mixture of Hydrodynamically Coupled Microrotors

Kyongmin Yeo,[1,2] Enkeleida Lushi,[3] and Petia M. Vlahovska[3]
[1]IBM T.J. Watson Research Center, Yorktown Heights, New York 10598, USA
[2]Division of Applied Mathematics, Brown University, Rhode Island 02912, USA
[3]School of Engineering, Brown University, Rhode Island 02912, USA
(Received 10 October 2014; revised manuscript received 5 January 2015; published 5 May 2015)

We study, numerically, the collective dynamics of self-rotating nonaligning particles by considering a monolayer of spheres driven by constant clockwise or counterclockwise torques. We show that hydrodynamic interactions alter the emergence of large-scale dynamical patterns compared to those observed in dry systems. In dilute suspensions, the flow stirred by the rotors induces clustering of opposite-spin rotors, while at higher densities same-spin rotors phase separate. Above a critical rotor density, dynamic hexagonal crystals form. Our findings underscore the importance of inclusion of the many-body, long-range hydrodynamic interactions in predicting the phase behavior of active particles.

DOI: 10.1103/PhysRevLett.114.188301 PACS numbers: 82.70.Dd, 47.57.J-, 47.57.Qk, 83.10.Tv

Systems of motile and interacting units can exhibit nonequilibrium phenomena such as self-organization and directed motion at large scales [1]. Theoretical studies of active matter report clustering [2], phase separations [3–5], and rotating structures [6]. Some of these phenomena have been observed in experiments of bacterial suspensions [7] or chemically activated motile colloids [8].

The collective motion of translating units such as bacteria has received much interest [1]. On the other hand, little is known about spinning units, partly because such systems were realized experimentally only recently. Active rotation of particles can be achieved using external forcing such as rotating magnetic fields [9,10], uniform electric fields (the Quincke rotation effect) [11], or chemical reactions [12]. Self-assembly from polymers by motile bacteria can create microrotors [13]. In biological systems, the dancing volvox [14], uniflagellar algae *C. reinhardtii* [15], and bacteria *T. majus* [16] exhibit rotorlike behaviors. Rising interest in rotor systems generated theoretical studies exploring rotor pair dynamics [17,18], nonequilibrium structure formation [19], dynamics at interfaces [20,21], rheology of suspensions [22,23], and phase separation driven by active rotation [24,25].

Models of the collective behavior of active matter often neglect particle motion due to the flow stirred by the other particles [4,5,24,26], tacitly assuming that the observed phase behavior of the "dry" system would persist in a system with fluid motion. However, in the viscosity-dominated world of colloidal-size particles, hydrodynamic interaction generates a long-range correlation, which can play an important role in the self-organization in many-body systems [27–29]. For example, in the studies of microswimmers, it was found that the hydrodynamic interactions determine the collective motion of squirmers (self-propelled spheres with no aligning interaction) [30] and the recently observed self-organization of bacteria into a macroscale bidirectional vortex when confined inside a drop [31] can only be explained by accounting for the fluid-mediated interactions [32]. It is the hydrodynamic interactions that cause two point rotors spinning in the opposite direction to translate [18] or undergo complex motions [33], instead of remaining fixed in space [24]. While the importance of hydrodynamic interactions in microswimmers (linearly propelled units) has been appreciated, large and dense populations of rotors have not been studied and the robustness of observed phase behavior in the dry spinner system [24] remains an open question.

In this Letter, we show that the hydrodynamic interactions between self-rotating nonaligning spherical particles have profound effects on self-organization. We consider monolayer suspensions of spherical rotors with clock- and counterclockwise spins suspended in liquid in a 3D domain [34]. At low densities, Fig. 1(a), a gaslike phase is observed with the rotors moving randomly in the stirred fluid. In contrast, in a dry system the spinners remain fixed in place (the frozen state in Ref. [24]). As the particle density further increases, a phase-separated fluid state emerges [Figs. 1(b) and 1(c)] with large clusters of same-spin rotors manifesting as lanes or macroscopic vortical structures. Past a critical particle density, dynamic crystals composed of both types of rotors emerge, Fig. 1(d).

Particle motions.—We consider microrotors whose size is such that inertia is negligible (overdamped or Stokes flow regime), under the assumption of strong convection by the fluid flow. A rotor centered at $\mathbf{x}_i$ with radius a subjected to a torque $\mathbf{T}$ generates a rotlet disturbance fluid flow $\mathbf{u}_R(\mathbf{x},\mathbf{x}_i) = \mathbf{T}\times(\mathbf{x}-\mathbf{x}_i)a^3/|\mathbf{x}-\mathbf{x}_i|^3$ with velocity decaying slowly with the distance from the rotor as $\sim 1/r^2$. The flow stirred by each rotor drags other rotors into motion. This is the essence of hydrodynamic interactions—a particle translates and rotates in response to the fluid flow generated by the motion of another particle. The rotors' positions and rotations evolve as [34]

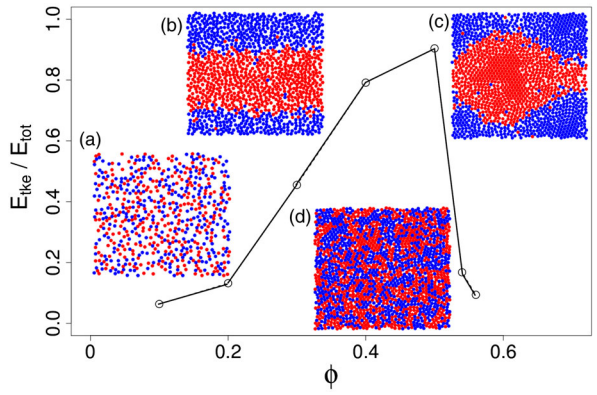

FIG. 1 (color online). The ratio of the translational kinetic energy to the total kinetic energy $\kappa = E_{\rm tke}/E_{\rm tot}$ as a function of rotor density ϕ. The insets are snapshots of simulations (50–50 mixture of clockwise(blue)—counterclockwise(red) spinning rotors) with total density (a) $\phi = 0.20$, (b) 0.40, (c) 0.50, and (d) 0.54. Movies are available in the Supplemental Material [34].

$$\frac{d\mathbf{x}_i}{dt} = \sum_{j\neq i}\left[\mathbf{u}_R(\mathbf{x}_i,\mathbf{x}_j) + O\left(\frac{a^7}{r^7}\right)\right] + \sum_{j\neq i}\mathbf{F}^S_{ij},$$
$$\Omega_i = \Omega_{0i} + \frac{1}{2}\nabla\times\mathbf{u}_R + O\left(\frac{a^8}{r^8}\right). \quad (1)$$

$\mathbf{F}^S_{ij}$ are (purely repulsive) steric or excluded volume interactions between the particles. $\Omega_0 = |\mathbf{T}|/8\pi\mu a^3$ is the rotation rate of an isolated rotor. Noise is neglected in Eq. (1), under the assumption of strong convection by the fluid flow $a^2\Omega_0/D_p \gg 1$ (D_p is the particle diffusivity); for colloidal rotors of radius 1 μm suspended in water this condition is met if $\Omega_0 > 0.01\ \mathrm{s}^{-1}$, which is well below experimentally observed values [12].

In dilute suspensions, where rotors are widely separated, the collectively generated fluid flows are well described by a superposition of the rotlet flows. However, in dense suspensions the full hydrodynamic interactions and the inclusion of closer-range lubrication flows become complicated to resolve analytically and require the use of sophisticated numerical methods.

The full hydrodynamic interactions between the rotors are computed using the force-coupling method. The long-range multibody interactions are fully resolved by solving the Stokes equations with regularized low-order multipoles, while the short-range lubrication interactions are included from analytical solutions [39]. The force-coupling method has been successfully applied to study suspension flows [40,41]. For a description of the numerical method see the Supplemental Material [34] and references therein.

The numerical simulations of the monolayer suspensions are performed in a computational domain of $H_x \times H_y \times H_z = 80a \times 20a \times 80a$, in which a is the particle radius and y denotes the direction in which torques are applied. Periodic boundary conditions are used in the x and z directions. The particle monolayer is located at $y = 0$ and the computational box is bounded by rigid walls located at $y = \pm H_y/2$. The vertical separation is chosen big enough to guarantee that the wall boundary does not affect the monolayer dynamics. Note that the rotors remain in the monolayer because the flow generated by their self-rotation does not induce particle translation in a direction normal to the monolayer [42].

We consider a 50:50 mixture of opposite-spin rotors with a total volume fraction varying from $\phi = 0.1$ to 0.56. For the monolayer suspension, the volume fraction is defined as $\phi = (\frac{4}{3}\pi a^3)N_p/(H_x \times H_z \times 2a)$, in which N_p is the number of the rotors. The number of suspended rotors varies from $N_p = 306$ at $\phi = 0.1$ to $N_p = 1,712$ at $\phi = 0.56$. To model the active rotation, external torques are applied to the rotors in the y direction. The magnitude of the external torque is normalized by the fluid viscosity μ_0 and the reference angular velocity Ω_0, $T^* = T/8\pi\mu\Omega_0 a^3 = \pm 1$. All of the simulations start from initial random configurations, generated by a molecular dynamics procedure. The dynamics are studied after the suspensions reach stationary states, typically about $t \simeq O(10^4)$ from the initial random state (time is nondimensionalized by Ω_0).

Hydrodynamic interactions and translation of rotors.—Since dynamics here is overdamped and not noisy, the system behavior is controlled by only one parameter, the rotor density ϕ. To assess the effect of the hydrodynamic interactions, we examine the conversion to translational kinetic energy ($E_{\rm tke}$) of the rotational kinetic energy ($E_{\rm rke}$) supplied to the suspension by the applied torque as rotor density increases. In the absence of hydrodynamic interactions, the rotors will remain fixed in space until random close packing is reached ($\phi_{\rm rep} \sim 0.56$) [43]. The flow generated by the rotating spheres moves them around and hinders their spinning [34]. Accordingly, the translational kinetic energy is expected to increase with particle density. However, Fig. 1 shows that the energy balance at steady state $\kappa = E_{\rm tke}/E_{\rm tot}$, where $E_{\rm tot} = E_{\rm rke} + E_{\rm tke}$, depends nonmonotonically on the rotor density.

Initially, as the particle separation decreases with ϕ, the hydrodynamic interactions become stronger thereby increasing κ. In contrast to the dry 2D gear-rotor system in which κ remains smaller than 2/3 [24], the equilibrium value set by equipartition, κ here becomes larger than 2/3 for $\phi = 0.40$ and 0.50 as the suspensions phase separate. In the phase-separated fluid regime, the suspensions develop large-scale collective motions, which contribute to the increase of $E_{\rm tke}$. As the system approaches random close packing, κ peaks at $\phi \simeq 0.50$ and decreases sharply afterwards, indicating a possible phase transition and change in the suspension microstructure. The κ peak occurs prior to random close packing due to lubrication effects: the strong hydrodynamic resistance generated by the flow in the thin gap between particles effectively locks the rotors together leading to coherent motion.

The changes in suspension structure are also suggested by the behavior of the mean-squared rotors' displacement $\mathrm{MSD} = \langle|\mathbf{x}_i(t) - \mathbf{x}_i(0)|^2\rangle/a^2$, shown in Fig. 2(a).

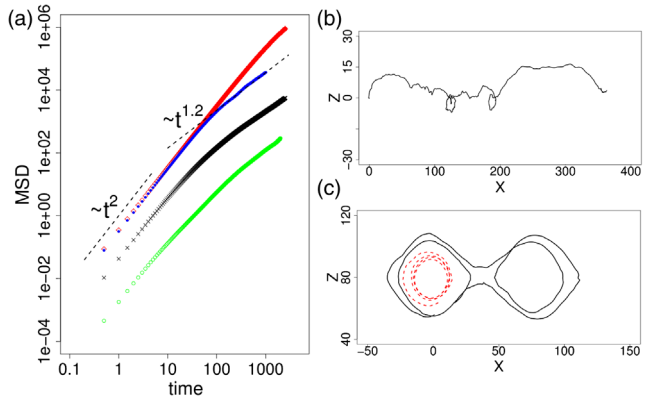

FIG. 2 (color online). (a) MSDs for $\phi = 0.2$ (times), 0.4 (diamond), 0.5 (closed circle), 0.56 (open circle). Representative trajectories for (b) $\phi = 0.40$, (c) 0.50. The red and black lines refer to trajectories of different rotors.

Hydrodynamic interactions give rise to random rotor motion, which in the short-time limit exhibits the typical ballistic $\sim t^2$ behavior. However, at intermediate times $100 < t < 1000$, the MSD changes from diffusion $\sim t$ at $\phi = 0.2$ to superdiffusion at $\phi = 0.4$ and 0.5. At short time scale, the MSDs for $\phi = 0.4$ and 0.5 are almost the same, as both systems are in the phase-separated fluid states. In the long-time limit, however, the MSD depends on the large-scale collective motion. For $t > 50$, the MSD for $\phi = 0.4$ grows at a much faster rate than $\phi = 0.5$. The superdiffusivity is due to Lévy flights of the rotors [44] seen in Figs. 2(b) and 2(c). The trajectories show that at $\phi = 0.4$ individual rotors move longer distances and circulate less in the macroscopic vortices compared to $\phi = 0.5$. At $\phi = 0.56$, the MSD is dramatically reduced due to crystal formation. Unlike to the dry gearlike rotor system [24], caging is not obvious in the MSD.

Spin segregation.—In the range of densities below the sharp drop in κ (i.e., $\phi \leq 0.5$), the rotors form dynamic assemblies [34] which in Figs. 1(b) and 1(c) are indicated as "phase-separated fluid." To quantify this tendency to cooperative motion we compute the number densities of the opposite-spin and same-spin rotors within distance r

$$\lambda^{\pm}(r) = \left\langle \frac{1}{N} \sum_{i=1}^{N} \left\{ \frac{\sum_{j=1, j\neq i}^{N} H(r - |\boldsymbol{d}_{ij}|)\delta(T_i \pm T_j)}{n\pi r^2 (2a)} \right\} \right\rangle.$$

$H(x)$ is the Heaviside function, $\delta(x)$ is the Dirac measure, N is the number of the suspended rotors, $|\boldsymbol{d}_{ij}|$ is the distance between the ith and jth rotors, and n is the number density. $\lambda^{\pm}$ are related to the pair distribution functions, $g_{AA}(r)$ and $g_{AB}(r)$ as $\lambda^{-}(r) \sim \int (g_{AA}) r dr$ and $\lambda^{+}(r) \sim \int (g_{AB}) r dr$; it can be interpreted as the average number of coherently moving neighbors [45].

Figure 3(a) illustrates $\lambda^{\pm}$ for $\phi = 0.5$. $\lambda^{-}(r)$ exceeds $\lambda^{+}(r)$ at small separations r implying clustering of the same-spin rotors. In the far field ($r > 30a$), eventually the number densities of the same- and opposite-spin rotors become the same. The average cluster size can be

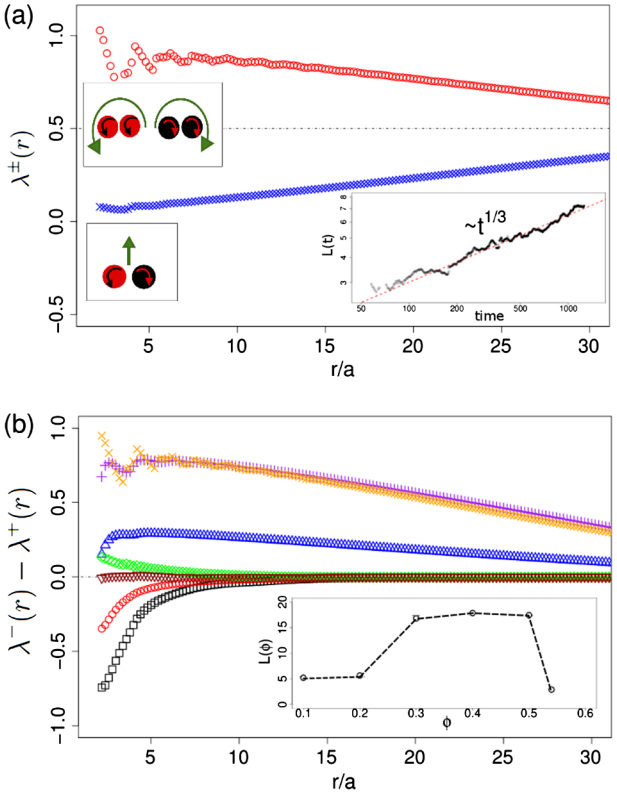

FIG. 3 (color online). (a) Normalized partial number density of same-spin (λ^{-}; ○) and opposite-spin (λ^{+}; ×) rotors for $\phi = 0.5$ at steady state. Insets illustrate co- and counterrotating particles and their joint rotation or translation. The inset shows a $\sim t^{1/3}$ growth of the length scale from the initial random configuration. (b) Average density difference between coherently moving same-spin and opposite-spin rotors, $\lambda^{-} - \lambda^{+}$, for $\phi = 0.1$ (square), 0.2 (circle), 0.3 (triangle), 0.4 (plus), 0.5 (times), 0.54 (diamond), and 0.56 (inverted triangle). The inset shows the final integrated length scale L as a function of ϕ.

characterized by the length scale over which the correlations between the rotors die out, $L(t) = \int r(\lambda^{-} - \lambda^{+}) dr / \int (\lambda^{-} - \lambda^{+}) dr$. Figure 3(a) shows that L grows as $\sim t^{1/3}$, which eventually saturates to the value shown in the inset of Fig. 3(b) (17.4 in this case). The exponent of $1/3$ is surprising as it is usually associated with coarsening dynamics in the absence of hydrodynamics. Hydrodynamic interactions are, however, known to give rise to diffusive behavior in suspension flows [46–48].

A more careful examination of the clustering shows that, in dilute suspensions ($\phi \leq 0.2$), rotors of opposite-spin tend to pair-up. Figure 3(b) shows that the difference between λ^{-} and λ^{+} reverses sign, indicating clustering of same-spin rotors, as the density increases above $\phi \sim 0.2$. The change of microstructure occurs because while at low densities the separation between rotors is large thereby allowing rotors to explore more space by translation (a pair of opposite spin rotors translates [34]), at higher densities assemblies that are less obstructing to the motion of other rotors are preferred (a pair of same spin rotors orbits around each other [34]). At $\phi = 0.4$ and 0.5, where complete separation

occurs, $\lambda^- - \lambda^+$ are almost identical for $r > 5a$. As ϕ increases further, $\phi \geq 0.54$, $\lambda^- - \lambda^+$ becomes close to zero, suggesting there is no or very weak preferential aggregation of the rotors. In the inset, L is shown as a function of ϕ. Spin segregation is captured by the integrated length scale which increases sharply at $\phi = 0.2$ and drops rapidly for $\phi \geq 0.54$.

Crystals.—At high density, rotors form crystals of hexagonal symmetry, see Fig. 4(a). The crystals are composed of rotors of either spin, and no spin segregation is observed for the duration of the simulations. The fraction of the crystal phase increases with density, and at $\phi = 0.56$ the crystal structure occupies roughly half of the computational domain. The formation of the crystals is tracked by an order parameter, $0 \leq \zeta_6 \leq 1$, which measures the average sixfold bond orientational order of the rotors;

$$\zeta_6 = \left\langle \frac{1}{N} \sum_i^N \left(\frac{1}{N_b} \sum_j^{N_b} e^{6\theta_{ij}\mathrm{i}} \right) \right\rangle.$$

θ_{ij} is the azimuthal angle of $\boldsymbol{d}_{ij}$ and N_b is the number of the neighboring rotors ($|\boldsymbol{d}_{ij}| < 2.05a$). ζ_6 is zero for an isotropic system and one for a perfect hexagonal crystal. Figure 4(b) shows that ζ_6 is almost zero up to $\phi = 0.5$ and increases rapidly from $\phi \simeq 0.54$, which corresponds with where the sudden drop of κ occurs (see Fig. 1).

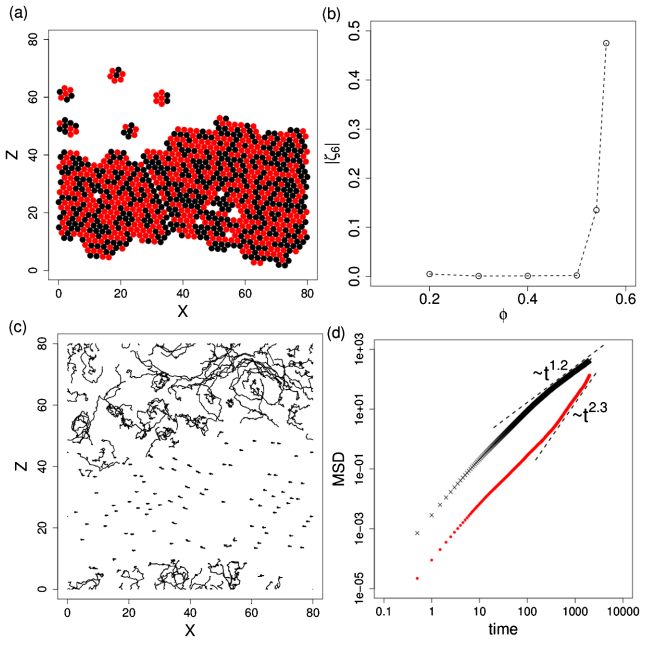

FIG. 4 (color online). (a) Crystal structures formed in a suspension at $\phi = 0.56$. The black and red circles denote the rotors rotating clockwise and counterclockwise, respectively. Note that for clarity only the rotors in crystals are shown. (b) Hexagonal bond-orientational order parameter ζ_6 as a function of ϕ. (c) Sample trajectories for $t = 0 \sim 600$ for $\phi = 0.56$. (d) MSDs of the rotors initially in crystal (closed circle) and in fluid regions (times).

Interestingly, even in the presence of crystals the rotors exhibit superdiffusive behavior with an exponent $\sim t^{1.2}$ at the intermediate time scale, see Fig. 2(a). Figure 4(c) illustrates trajectories of 170 randomly selected rotors. Particle mobility is much lower in the crystal region than in the fluid region: even though the trajectories are shown for a relatively long period $t = 0 \sim 600$, rotors located in a crystal move only very short distance, usually less than a particle diameter, while rotors in the fluid region travel considerably longer distance ($> 15a$). The difference in mobilities is also evident from Fig. 4(d), which compares the MSDs for the rotors initially in a crystal and in a fluid region. The MSD for the rotors in a crystal grows very rapidly $\sim t^{2.3}$ for $t > 400$. The rapid growth of the MSD seems related to structural rearrangements, i.e., large-scale motions of crystal and escape of the rotors in the crystal to the fluid region. Note that the crystal structure dynamically melts, reassembles, and moves, see movies in Ref. [34].

Conclusions and outlook.—Suspensions of active particles exhibit complex phase behavior [1] and self-translating particles have attracted extensive studies [3,4,30,45]. Here we show that self-rotating particles are driven by hydrodynamic interactions into mobile clusters and crystals even in the absence of self-propulsion or ambient flows. The resulting collective dynamics is very different from that observed in a dry system [24].

The effect of the hydrodynamic interactions is assessed by observing the conversion rate of the rotational to the translational kinetic energies (κ). κ initially increases with the rotor density, and eventually exhibits a sudden drop at $\phi \simeq 0.54$. For $\phi \geq 0.54$, the active rotors start to form crystal structures, which are responsible for the sudden drop of κ. In contrast, the dry, no-noise system of gearlike rotors [24] exhibits $\kappa = 0$ (in the frozen state) followed by monotonic increase of κ above a critical density ϕ_c corresponding to about 0.5 in our notation. We found that the opposite-spin rotors tend to stay close at low ϕ, whereas for $\phi > 0.2$ separation into fluid phases of same-spin rotors occurs. All of these suggest that multibody hydrodynamic interactions play a significant role in the collective dynamics and phase behavior of suspensions of active rotors and these effects should not be neglected in studies of similar active systems. For example, hydrodynamic interactions could influence or drive the formation of the peculiar dynamical structures experimentally observed at the interface of drops covered with colloidal particles [49,50].

In this Letter we considered only torques that are perpendicular to the particle monolayer. Because of the symmetry of the generated flows, the particles remain confined to the monolayer and do not move transversely. In experimental systems, for example Quincke rotors [51,52], it is not the case that torques stay in one direction or even constant, as the particle rotation is dependent on the full electrohydrodynamics. Although restricting the rotational motion to one direction in experiments is challenging, it is not impossible and our study suggests potentially intriguing

experiments. Another problem that remains relatively unexplored is that of using spinners and rotors for transport and mixture of passive particles [24]. Finally, this work with rotor monopoles serves as a solid basis to treat rotor dipoles, which are commonly encountered in biology, e.g., swimming bacteria with rotating flagella or a cytoskeletal torque dipole consisting of two actin filaments and myosin motors [53].

E. L. and P. V. acknowledge support from the NSF through CBET Grant No. 1437545.

[1] M. C. Marchetti, J. F. Joanny, S. Ramaswamy, T. B. Liverpool, J. Prost, M. Rao, and R. A. Simha, Rev. Mod. Phys. **85**, 1143 (2013).
[2] F. Peruani, A. Deutsch, and M. Bar, Phys. Rev. E **74**, 030904 (2006).
[3] Y. Fily and M. C. Marchetti, Phys. Rev. Lett. **108**, 235702 (2012).
[4] G. S. Redner, M. F. Hagan, and A. Baskaran, Phys. Rev. Lett. **110**, 055701 (2013).
[5] J. Stenhammar, A. Tiribocchi, R. J. Allen, D. Marenduzzo, and M. E. Cates, Phys. Rev. Lett. **111**, 145702 (2013).
[6] H. H. Wensink, V. Kantsler, R. E. Goldstein, and J. Dunkel, Phys. Rev. E **89**, 010302(R) (2014).
[7] H. P. Zhang, A. Beer, E.-L. Florin, and H. L. Swinney, Proc. Natl. Acad. Sci. U.S.A. **107**, 13626 (2010).
[8] J. Palacci, C. Cottin-Bizonne, C. Ybert, and L. Bocquet, Phys. Rev. Lett. **105**, 088304 (2010).
[9] B. S. Grzybowski, H. A. Stone, and G. M. Whitesides, Nature (London) **405**, 1033 (2000).
[10] B. A. Grzybowski and G. M. Whitesides, Science **296**, 718 (2002).
[11] A. Bricard, J. B. Caussin, N. Desreumaux, O. Dauchot, and D. Bartolo, Nature (London), **503**, 95 (2013).
[12] Y. Wang, S. Fei, Y.-M. Byun, P. E. Lammert, V. H. Crespi, A. Sen, and T. E. Mallouk, J. Am. Chem. Soc. **131**, 9926 (2009).
[13] J. Schwarz-Linek, C. Valeriani, A. Cacciuto, M. E. Cates, D. Marenduzzo, A. N. Morozov, and W. C. K. Poon, Proc. Natl. Acad. Sci. U.S.A. **109**, 4052 (2012).
[14] K. Drescher, K. C. Leptos, I. Tuval, T. Ishikawa, T. J. Pedley, and R. E. Goldstein, Phys. Rev. Lett. **102**, 168101 (2009).
[15] J. Guasto, V. Kantsler, and M. Polin (private communication). A typically biflagellate algae such as Chlamydomonas reinhardtii exhibits mostly rotational motion when one of the flagella is removed.
[16] A. Petroff, X.-l. Wu, and A. Libchaber, Phys. Rev. Lett. **114**, 158102 (2015)
[17] M. Leoni and T. B. Liverpool, Europhys. Lett. **92**, 64004 (2010).
[18] Y. Fily, A Baskaran, and M. C. Marchetti, Soft Matter **8**, 3002 (2012).
[19] E. Climent, K. Yeo, M. R. Maxey, and G. E. Karniadakis, J. Fluids Eng. **129**, 379 (2007).
[20] I. Llopis and I. Pagonabarraga, Eur. Phys. J. E **26**, 103 (2008).
[21] P. Lenz, J.-F. Joanny, F. Julicher, and J. Prost, Phys. Rev. Lett. **91**, 108104 (2003).
[22] K. Yeo and M. R. Maxey, Phys. Rev. E **81**, 062501 (2010).
[23] L. Jibuti, S. Rafaï, and P. Peyla, J. Fluid Mech. **693**, 345 (2012).
[24] N. H. P. Nguyen, D. Klotsa, M. Engel, and S. C. Glotzer, Phys. Rev. Lett. **112**, 075701 (2014).
[25] Y. Goto and H. Tanaka, Nat. Commun. **6**, 5994 (2015).
[26] R. Ni, M. A. C Stuart, and M. Dijkstra, Nat. Commun. **4**, 2704 (2013).
[27] A. Campa, T. Dauxois, and S. Ruffo, Phys. Rep. **480**, 57 (2009).
[28] M. Baron, J. Blawzdziewicz, and E. Wajnryb, Phys. Rev. Lett. **100**, 174502 (2008).
[29] I. Shani, T. Beatus, R. H. Bar-Ziv, and T. Tlusty, Nat. Phys. **10**, 140 (2014).
[30] A. Zöttl and H. Stark, Phys. Rev. Lett. **112**, 118101 (2014).
[31] H. Wioland, F. G. Woodhouse, J. Dunkel, J. O. Kessler, and R. E. Goldstein, Phys. Rev. Lett. **110**, 268102 (2013).
[32] E. Lushi, H. Wioland, and R. E. Goldstein, Proc. Natl. Acad. Sci. U.S.A. **111**, 9733 (2014).
[33] E. Lushi and P. M. Vlahovska, arXiv:1503.01805 [J. Nonlinear Sci. (to be published)].
[34] See Supplemental Material at http://link.aps.org/supplemental/10.1103/PhysRevLett.114.188301 for movies showing the dynamics at various particles densities, discussions on the nature of hydrodynamic interactions, description of the numerical method and other information, which includes Refs. [35–38].
[35] S. Kim and S. J. Karrila, *Microhydrodynamics: Principles and Selected Applications* (Butterworth-Heinemann, Boston, 1991).
[36] R. Schmitz and B. U. Felderhof, Physica (Amsterdam) **116A**, 163 (1982).
[37] H. Brenner, Annu. Rev. Fluid Mech. **2**, 137 (1970).
[38] S. Lomholt and M. R. Maxey, J. Comput. Phys. **184**, 381 (2003).
[39] K. Yeo and M. R. Maxey, J. Comput. Phys. **229**, 2401 (2010).
[40] E. Climent, M. R. Maxey, and G. E. Karniadakis, Langmuir **20**, 507 (2004).
[41] K. Yeo and M. R. Maxey, J. Fluid Mech. **649**, 205 (2010).
[42] Note that even though each rotor particle moves only within the monolayer, mimicking a 2D system, the particle motion is affected by the full 3D hydrodynamic interactions though the embedding fluid, i.e., the flows in the fluid space above and below the monolayer.
[43] For a monolayer, random close packing is set by the rotors' cross-sectional area fraction $\phi_A \sim 0.84$. $\phi = \phi_A 2/3$.
[44] T. H. Solomon, E. R. Weeks, and H. L. Swinney, Phys. Rev. Lett. **71**, 3975 (1993).
[45] A. Wysocki, R. G. Winkler, and G. Gompper, Europhys. Lett. **105**, 48004 (2014).
[46] A. Sierou and J. F. Brady, J. Fluid Mech. **506**, 285 (2004).
[47] K. Yeo and M. R. Maxey, Europhys. Lett. **92**, 24008 (2010).
[48] R. H. Davis, J. Fluid Mech. **310**, 325 (1996).
[49] P. Dommersnes, Z. Rozynek, K. Kjerstad, R. Castberg, A. Mikkelsen, K. Hersvik, and J. O. Fossum, Nat. Commun. **4**, 2066 (2013).
[50] M. Ouriemi and P. M. Vlahovska, J. Fluid Mech. **751**, 106 (2014).
[51] P. F. Salipante and P. M. Vlahovska, Phys. Rev. E **88**, 043003 (2013).
[52] D. Das and D. Saintillan, Phys. Rev. E, **87**, 043014 (2013).
[53] S. Fürthauer, M. Strempel, S. W. Grill, and F. Julicher, Phys. Rev. Lett. **110**, 048103 (2013).